Soils and Rocks
An International Journal of Geotechnical and Geoenvironmental Engineering
www.soilsandrocks.com
ISSN 1980-9743
ISSN-e 2675-5475

Shear strength of expansive soils under different moisture conditions: a comparative evaluation of laboratory and in-situ test methods for slope stability design

Jingjing Li[1#], Lingwei Kong[2], Lei Jin[1], Xinming Li[2,3]

Article

Keywords
Expansive soil
Shear strength
Flooding
Borehole shear test
Slope stability

Abstract

Expansive soils are prone to strength degradation after rainfall, yet conventional slope stability analyses often rely on laboratory-derived shear strength parameters that may overestimate in-situ conditions. This study evaluates and compares the shear strength of expansive soils using the borehole shear test (BST), laboratory direct shear test (DST), and consolidated undrained test (CUT) under natural and flooding conditions. Results show that shear stress- shear displacement (or axial strain) curves generally exhibit weak hardening characteristics. Significant reductions in cohesive strength occur after flooding. The cohesive force obtained by DST and BST decreases by 18.2 kPa and 13.1 kPa after flooding respectively, while the internal friction angle decreases slightly within 3°. Laboratory tests consistently yield higher strength parameters than BST, while flooding BST values closely align with those measured on actual slip surfaces. Numerical modeling of an unstable cut slope confirms that using flooding BST parameters produces more realistic safety factors. The findings highlight the importance of incorporating in-situ testing under representative moisture conditions for reliable slope stability design in expansive soils.

1. Introduction

Expansive soils are widely recognized as a "prevalent engineering issue" due to their swelling-shrinkage behavior, which can lead to significant geotechnical hazards such as slope instability, ground heave, and structural damage. These soils are extensively distributed across more than 20 provinces in China (Shi et al., 2002; Pei et al., 2020; Li & Kong, 2021; Dai et al., 2024), as well as in many other countries including the United States, India, and Tunisia. Landslides frequently occur on expansive soil slopes. Notable examples include the Houba landslide in the Three Gorges Reservoir Area, China (Hou et al., 2013); landslides along national roads in Béja, Tunisia (Jamei et al., 2015); 19 landslides occurring along the Nanyang section of the South-to-North Water Diversion Project in China (Dai et al., 2017); and landslides affecting the Yanji-Hunchun High-speed Railway in northeast China (Kong et al., 2018).

Despite the fact that expansive soils typically exhibit relatively high peak shear strength under laboratory conditions, field observations indicate that the actual shear strength mobilized during slope failures is often significantly lower than the measured peak values (Lin et al., 2002; Cheng et al., 2011; Liu et al., 2011). This discrepancy has raised concerns among researchers and engineers regarding the accuracy and applicability of conventional strength parameters in slope stability analyses involving expansive soils.

Environmental factors play a crucial role in the progressive degradation of expansive soil slopes. Due to exposure to atmospheric forces, such as evaporation and precipitation, cracks and fissures gradually develop within the active zone of these slopes (Nelson & Miller, 1992; Cheng et al., 2011). Hou et al. (2013) believed that the dry and wet cycle was the main reason for the progressive failure of expansive soil slope. Zhang et al. (2023) conducted numerical simulations to access the combined effects of expansion force and dry-wet cycles on slope stability. Their findings revealed that while the expansion force may reduce the safety factor prior to environmental cycling, it is the cumulative effect of dry-wet cycles that predominantly triggers shallow instability in expansive soil slopes. Conversely, Cheng et al. (2011) suggested that although the dry-wet cycle could compromise soil structure, its strength remained high, indicating that this cycle might not be the principal cause of slope instability.

#Corresponding author. E-mail address: lijingjing@jsou.edu.cn
[1]Jiangsu Open University, College of Civil Engineering, Nanjing, China.
[2]Chinese Academy of Sciences, Institute of Rock and Soil Mechanics, State Key Laboratory of Geomechanics and Geotechnical Engineering Safety, Wuhan, China.
[3]Zhongyuan University of Technology, School of Civil Engineering and Architecture, Zhengzhou, China.

Submitted on August 20, 2024; Final Acceptance on March 20, 2026; Discussion open until November 30, 2026.
Editor: Renato P. Cunha
https://doi.org/10.28927/SR.2026.006424

In addition to dry-wet cycles, seasonal variations in temperature and humidity, such as freeze-thaw cycles, are also known to exacerbate the deterioration of expansive soil slopes, particularly in colder regions like northeast China (Kong et al., 2018).

Given the unsaturated nature of the near-surface layers of expansive soil slopes, considerable attention has been given to understanding the influence of matric suction and saturation on soil strength from the perspective of unsaturated soil mechanics (Zhang et al., 2020; Niu et al., 2024; Luo et al., 2024). Rainfall infiltration further complicates the hydro-mechanical response of expansive soils, leading to pore pressure buildup, reduction in effective stress, and consequent loss of strength. Numerous studies have investigated the impact of rainfall-induced infiltration on slope stability (Zhan et al., 2007; Xu et al., 2014; Dai et al., 2017; Liang et al., 2021; Chang et al., 2022; Hou et al., 2023), particularly since most expansive soil slope failures occur during or shortly after rainy periods.

Conventional stability analyses typically rely on strength parameters from laboratory direct shear or triaxial tests. However, increasing evidence suggests that relying solely on laboratory-derived parameters may not adequately represent the in-situ mechanical behavior of expansive soils. Field test methods, such as in-situ direct shear tests, borehole shear tests, pressuremeter tests, standard penetration tests, and dilatometer tests, have been employed to a limited extent in expansive soil areas (Kong et al., 2017; Luo et al., 2024; Marsland & Randolph, 1977; Li et al., 2024; Ng et al., 2003; Zhan, 2003; Ng & Zhan, 2007). Nevertheless, there remains a lack of comprehensive comparisons between in-situ and laboratory-measured strength parameters for expansive soils.

Notably, conflicting results have emerged from different studies. For instance, Yang et al. (2014) reported that in-situ direct shear test results yielded higher shear strength values compared to laboratory tests, whereas Liu et al. (2011) observed the opposite trend. Such discrepancies highlight the challenges faced by geotechnical designers when selecting appropriate strength parameters for practical applications. Given the complex behavior of expansive soils, where cracking, cyclic wetting-drying, and water infiltration progressively degrade soil strength, it is imperative to adopt a multi-method approach for evaluating shear strength characteristics.

This study aims to address these gaps through a comparative analysis of shear strength using three different test methods: in-situ borehole shear tests, laboratory direct shear tests, and consolidated undrained triaxial tests. Tests were performed under varying hydraulic conditions to investigate how moisture content and test method influence strength characteristics. Based on the experimental results, a strength reduction method was performed on an actual unstable cut slope, providing practical insights for selecting appropriate strength parameters in expansive soil engineering.

2. Geotechnical and geologic properties

The field investigations were conducted on an expansive soil slope in the Nanyang Basin, Henan Province, China (Figure 1).

The cut slope under investigation has a height of approximately 6.0 m. A representative expansive soil layer was selected for drilling and sampling. Within the investigated depth range, the soil between 1.0 and 2.0 m exhibits an ochreous color, while the soil from 3.0 to 6.0 m appears reddish-brown. Manganese and calcareous nodules are present throughout all soil layers. No groundwater was encountered within the investigation depth, which extended to a maximum of 10.0 m. The temperature during testing was around 30°C.

The tested soils were collected from the expansive soil slope at depths of 2.0-6.0 m using pit exploration. Basic physical properties were determined according to the Chinese standard JTG 3430-2020 (JTG, 2020), as presented in Table 1. The properties of the soil at a depth of 2.0 m are listed separately, as they differ significantly from those at other depths. In contrast, the physical properties of the soils between 3.0 m and 6.0 m are largely consistent. According to the Unified Soil Classification System (ASTM D2487-17) (ASTM, 2017), the plastic limit (w_P), liquid limit (w_L), and plasticity index (*PI*) indicate that the soil at 2.0 m is classified as low plasticity clay, while the soil at 3.0-6.0 m is categorized as high plasticity clay. The measured liquidity index (*LI*) values indicate that the soil at 2.0 m is in the hard state, whereas the soil at 3.0-6.0 m is in a hard plastic or hard state, according to the Chinese standard JTG 3363-2019 (JTG, 2019). The activity (A_c) ranges between 0.75 and 1.25, classifying the soil as “normal” clay (Nelson et al., 2015). Additionally, based on the Chinese standard JTG C20-2011 (JTG, 2011) for expansive soil classification, the free-swell value (F_s) and standard absorption moisture content (ω_f) indicate low expansiveness at 2.0 m and medium-level expansiveness at 3.0-6.0 m. Figure 2 shows the particle size distribution curves of the expansive soils. Particles smaller than 5.0 μm account for 35.8% of the soil at 2.0 m and 44.8% at 3.0-6.0 m, indicating a high clay fraction.

Table 1. Physical property parameters of expansive soils.

Physical properties	Depth, z (m)	
	2.0	**3.0-6.0**
Water content, ω (%)	24.2	25.5-26.9
Density, ρ (g/cm^3)	1.88	1.96-1.98
Specific gravity, G_s	2.72	2.71
Saturation, S_r (%)	82.6	94.0-96.3
Free-swell value, F_s (%)	56	62-66
Plastic limit, w_P (%)	25.7	26.2
Liquid limit w_L (%)	49.2	55.4
Plasticity index, *PI* (%)	23.5	29.2
Liquidity index, *LI*	-0.06	-0.024-0.024
Activity, A_c	0.94	0.93
Standard absorption moisture content, ω_f (%)	4.2	6.7

Table 2. Mineral compositions of the expansive soil.

Quartz (%)	Feldspar (%)	Clay mineral (%)			
		Montmorillonite	Chlorite	Illite	Kaolinte
40	8	16	18	8	10

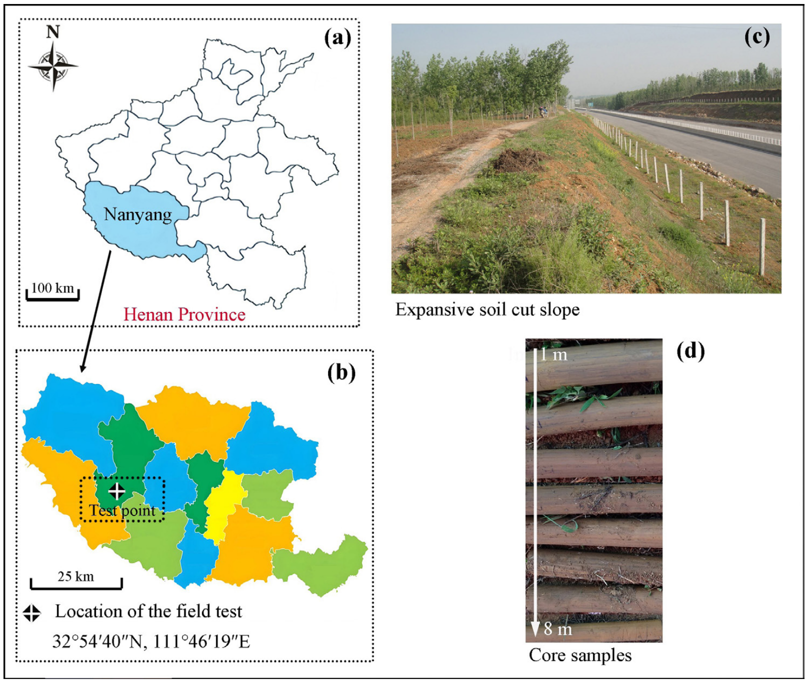

Figure 1. Study area location and representative core samples: (a) map of Henan Province, (b) detailed map of Nanyang City showing the field test site, (c) photograph of the expansive soil cut slope, and (d) core samples collected via drilling at the site.

Mineralogical composition was analyzed using an X'TRA-type X-ray diffractometer (Thermo Fisher Scientific, Switzerland) with Jade 5.0 software. The results, summarized in Table 2, show that the soil primarily consists of montmorillonite and chlorite, with minor amounts of illite and kaolinite, along with non-clay minerals such as quartz and feldspar.

3. Test scheme

To investigate the influence of flooding conditions and test methods on the shear strength behavior of Nanyang expansive soil, in-situ borehole shear tests (BST), laboratory direct shear tests (DST), and consolidated undrained triaxial tests (CUT) were conducted. Although using in-situ porewater or a chemically matched solution would better reflect field conditions, distilled water was used for saturation to ensure consistency across all three methods, as required by the constraints of the CUT apparatus. Laboratory tests were performed at a controlled temperature of 30°C ± 1°C.

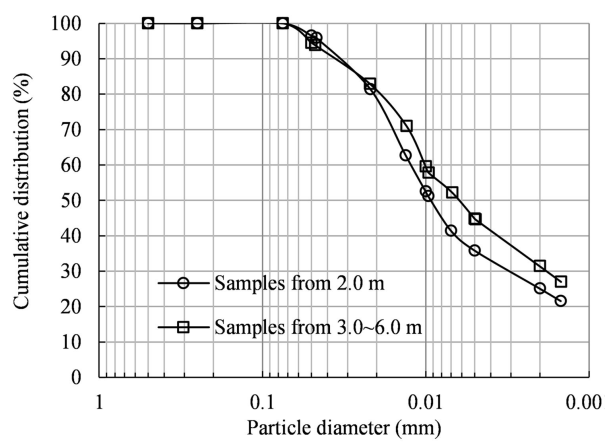

Figure 2. The particle size distribution curve of the expansive soil.

3.1 Borehole shear test

The BST device (Model No. A104.2) used in this study primarily comprises a control box, a shear disc, and a shear probe.

Figures 3 shows the borehole shear test apparatus and a schematic diagram of its testing system. Normal stress is applied using an external gas source, with a maximum capacity of 500 kPa, while the maximum achievable shear stress is 350 kPa. Tests were conducted in 75 mm-diameter boreholes. Consolidation time was set to 20 min after initial application of normal stress and reduced to 10 min for subsequent loading stages (Lutenegger & Hallberg, 1981; Yu et al., 2016). Shearing was performed at a constant rate of 0.05 mm/s.

BSTs were conducted in adjacent boreholes at depths of 3.0-6.0 m, spaced approximately 1.5 m apart. The procedure was as follows:

(1) A 75 mm- diameter borehole was drilled to the preset test depth.
(2) The shear probe was lowered to the target depth, and normal stress was applied vertically to the borehole wall using a gas cylinder connected through the control box.
(3) After sufficient consolidation under the applied normal stress, shear stress was induced by rotating the crank clockwise at a rate of approximately 2 revolutions per second (rps). During shearing, the shear gauge reading was monitored, and corresponding displacement and shear stress values were recorded.
(4) Cranking continued at 2 rps until peak shear stress was reached, indicating shear failure.
(5) The crank was reversed to return the base plate gauge reading to near zero. The gas pressure was then increased using the regulator, and steps 3 and 4 were repeated under the next normal stress level (see Table 3).
(6) After completing the tests at one depth, the borehole was deepened to the next test level, and steps 2-5 were repeated.
(7) For the flooding condition test, the borehole was immediately filled with water after drilling. To prevent excessive expansion or collapse of the borehole wall, the shear probe was quickly lowered to the test depth after flooding and left in place for 60 min to allow saturation. Steps 2-5 were then conducted under submerged conditions.

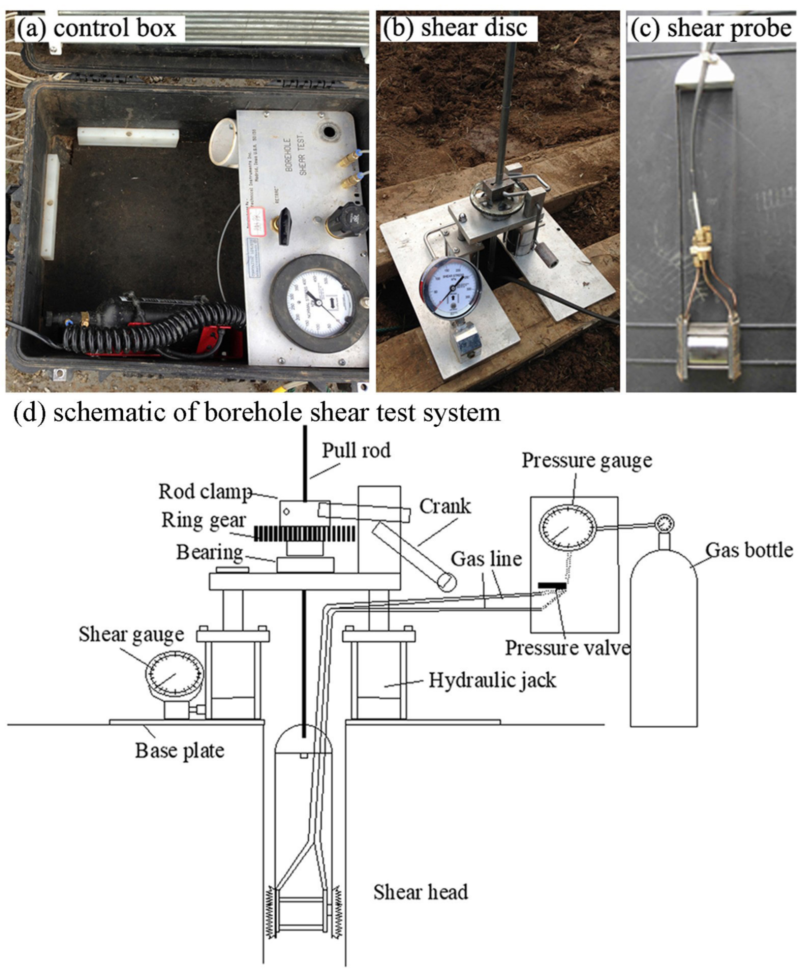

Figure 3. Device of borehole shear test and schematic of borehole shear test system: (a) control box, (b) shear disc, (c) shear probe, and (d) schematic of borehole shear test system.

3.2 Laboratory direct shear test

DSTs were conducted in accordance with the Chinese standard JTG 3430-2020 (JTG, 2020). Undisturbed cylindrical samples were prepared with a diameter of 61.8 mm and a height of 20 mm. The samples were divided into two groups, one tested at natural moisture content and the other fully saturated.

For the saturated group, samples confined within the sampling rings were placed in a sealed vacuum chamber. Air was evacuated for 4 hours, after which distilled water was gradually introduced under vacuum until the samples were fully submerged. They were then left immersed in distilled water for an additional 24 hours to ensure complete saturation. Throughout this process, radial deformation was constrained by the rigid sampling rings, while porous stones placed on both ends and the saturation fixture limited vertical movement. The degree of saturation was estimated from the measured water uptake during immersion.

Prior to consolidation, a thin layer of silicone grease was applied to the inner surfaces of the shear box to minimize boundary friction. Specimens were consolidated under the same normal stresses used in the BST (see Table 3) until the vertical deformation rate dropped below 0.005 mm/h. Shear loading was then applied at a constant rate of 0.8 mm/min. Distilled water was continuously supplied to the shear box during testing to maintain full saturation.

For the natural moisture content group, wet cotton was wrapped around the loading plate to prevent minimize loss during the test.

3.3 Consolidated undrained test

CUTs were conducted in accordance with the Chinese standard JTG 3430-2020 (JTG, 2020). Undisturbed cylindrical samples, with a diameter of 39.1 mm and a height of 80 mm, were secured in rigid saturators and saturated using the same procedure as in the DSTs.

After saturation and dimensional measurement, samples were placed in the triaxial cell. Back-pressure saturation was applied incrementally through the base until the pore-water pressure coefficient exceeded 0.98. Throughout this stage, a confining pressure 20 kPa higher than the back pressure was maintained to suppress swelling and preserve specimen integrity.

Consolidation was then performed under the isotropic confining pressures listed in Table 3, with drainage permitted. Both excess pore water pressure dissipation and drainage volume were continuously monitored, and consolidation was considered complete when more than 95% of the excess pore pressure had dissipated. The drainage valve was then closed to enforce undrained conditions, and undrained shearing was performed at a constant rate of 0.073 mm/min. Shearing continued until either a well-defined peak deviator stress was observed or axial strain reached 15-20%.

Experimental results from the BST, DST and CUT are comparatively analyzed in Section 4 to evaluate the influence of test method and moisture condition on the observed shear behavior.

4. Evaluation of shear strength behavior using different test methods

Figure 4 shows the shear stress-displacement curves from BST and DST, while Figure 5 presents the shear stress-axial strain, pore water pressure- axial strain, and shear stress-effective mean stress curves from CUT. As shown, the shear stress-shear displacement (or axial strain) curves generally exhibit weak hardening characteristics.

Table 3. Schemes of borehole shear test.

Normal stress (kPa)	Hydraulic condition
25,50,75,100,150,200,300,400	Non-flooding flooding

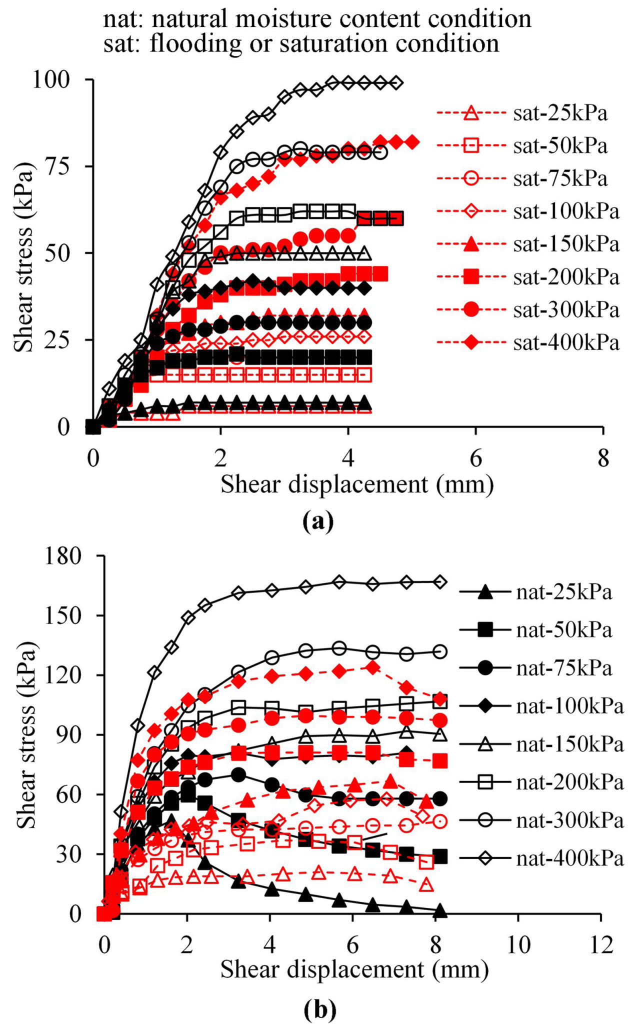

Figure 4. The shear stress - displacement relationship curves (a) from BST at 4.0 m; (b) from DST.

However, under natural moisture conditions, the shear stress-shear displacement curves from DST present softening behavior when the applied normal stress is less than 100 kPa. This phenomenon occurs because, at normal stresses below the in-situ horizontal stress of the soil, the soil behaves similarly to overconsolidated soil. Upon saturated, the soil experiences a form of stress release, effectively reducing the pre-consolidation effect and eliminating the softening deformation characteristics observed under natural moisture conditions.

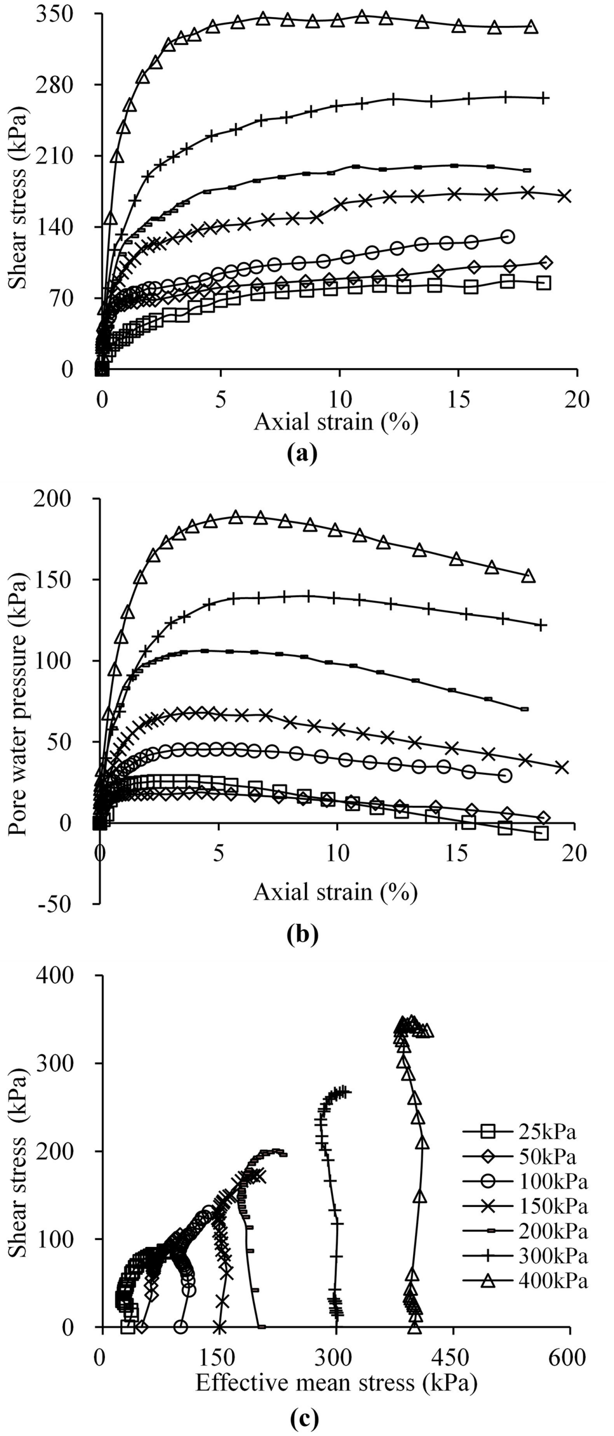

Figure 5. The shear stress (pore water pressure) - axial strain relationship curves from CUT: (a) The shear stress - axial strain relationship curves; (b) The pore water pressure - axial strain relationship curves; (c) The shear stress - effective mean stress relationship curves.

Figure 6 presents the strength envelope curves from BST, DST and CUT. As indicated by the non-flooding BST results, the failure envelope can be approximated by two linear segments. At lower normal stress levels, the failure envelope is relatively steep, whereas it becomes gentler when the normal stress exceeds a certain threshold.

Two possible explanations exist for this behavior. The first suggests that under low normal stress, the soil behaves in a drained manner during shearing. As the normal stress increases, the soil undergoes an undrained shear process, leading to the generation of positive pore water pressure. This reduces the effective stress and consequently lowers the shear strength, resulting in a flatter failure envelope. The second possibility is that under low normal stress, the shear plate does not embed effectively into the hard or overconsolidated soil, leading to an underestimation of the actual shear strength. As the normal stress increases, the shear plate becomes fully embedded, revealing the true strength of the soil.

The experimental results of this study align more closely with the second explanation. The expansive soil in the study area is overconsolidated and exists in a hard state. Under low normal stress, the shear plate is not fully embedded, resulting in lower measured strength values. A distinct break point in the failure envelope occurs at approximately 100 kPa normal stress. When the soil is saturated through flooding, the shear plate can embed completely even under low normal stress, and the resulting failure envelope exhibits a single linear trend. This phenomenon has been observed in previous studies (Lutenegger & Hallberg, 1981; Handy et al., 1985).

The failure envelopes obtained from DST and CUT also exhibit a bilinear trend, with a distinct break point occurring at normal stress (or confining pressure) levels of approximately 100 kPa and 120 kPa, respectively. The stress level at the intersection of the two-stage strength envelopes from all three test methods closely corresponds to the in-situ horizontal stress (S_H) values. These include a consolidation test-derived horizontal stress of 120 kPa (as shown in Figure 7), in-situ horizontal stress measurements ranging from 104.5 kPa to 107.2 kPa, and pressuremeter test results varying between 108.4 kPa and 127.4 kPa.

The shear strength parameters obtained from different test methods are summarized in Table 4. It is evident that hydraulic conditions have a significant effect on the shear strength of expansive soil, particularly in terms of the reduction in cohesive force (c) after flooding. The c values obtained from DST and BST decrease by 18.2 kPa and 13.1 kPa, respectively, after flooding, while the internal friction angle (φ) reduces slightly within 3°.

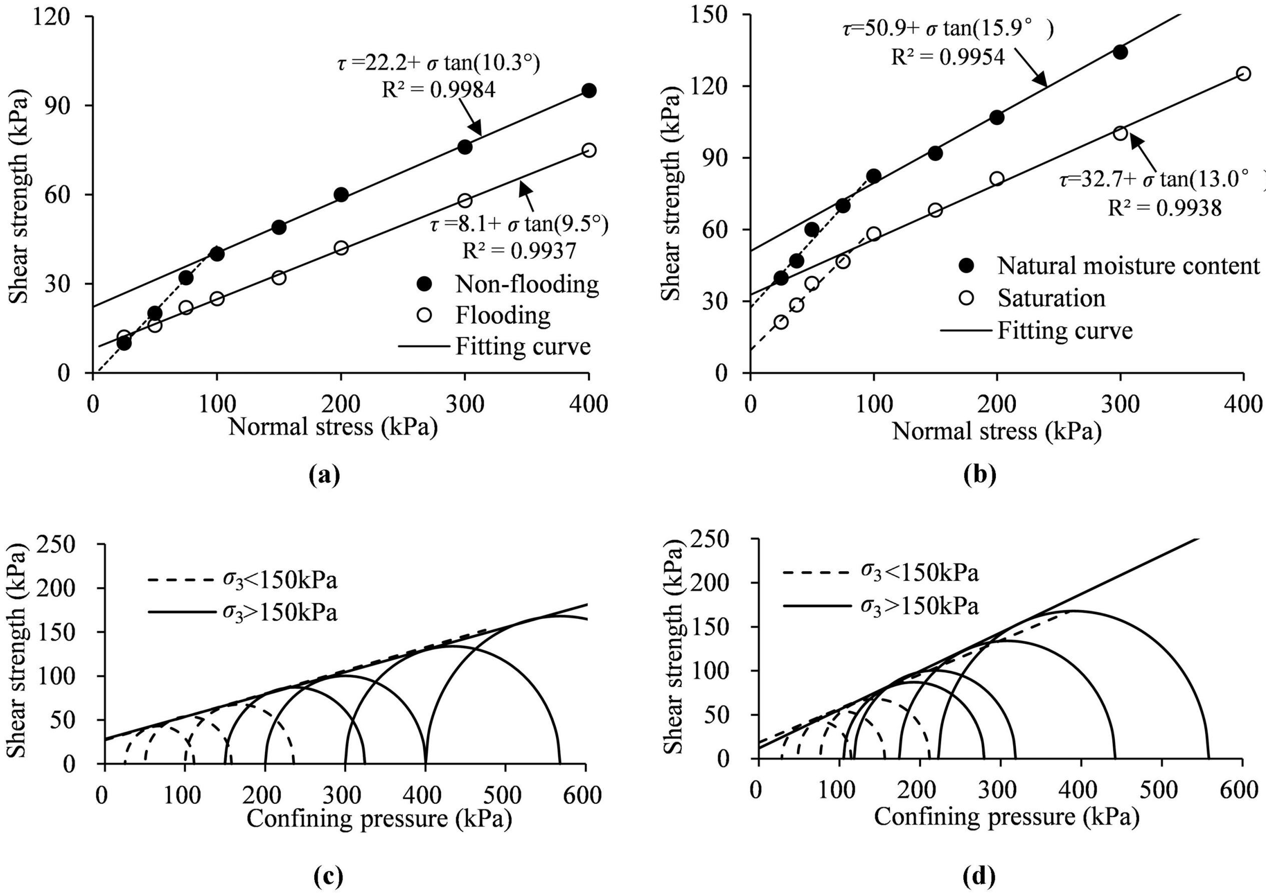

Figure 6. Strength envelope curves: (a) from BST at 3.0 m; (b) form DST; (c) total strength from CUT; (d) effective strength from CUT.

This reduction in c is primarily attributed to the presence of strong hydrophilic clay minerals in the studied soils. Upon flooding, water infiltration initiates hydration of the clay minerals, leading to an expansion of the double-layer water film around particles. This process disrupts the original clay particle arrangements and weakens the interparticle bonding, thereby reducing the cohesive strength. Moreover, the development of swelling-induced microcracks further deteriorates the soil structure, promoting changes in pore characteristics such as increased porosity and connectivity, which accelerate the loss of mechanical integrity. In contrast, the φ values exhibit only a slight decrease, which can be attributed to the soil's high initial degree of saturation (94%). Under such conditions, the additional lubrication effect between particles caused by water infiltration is minimal, limiting the reduction in shear resistance along sliding surfaces.

Among the test methods, DST yields the highest c values under identical hydraulic conditions. This is because the DST imposes a fixed shear plane during shearing, and the corresponding soil sample can be considered as an intact clod without pre-existing structural planes or fractures. In contrast, the samples tested in BST and CUT represent the natural soil mass, which generally has lower strength than intact clods.

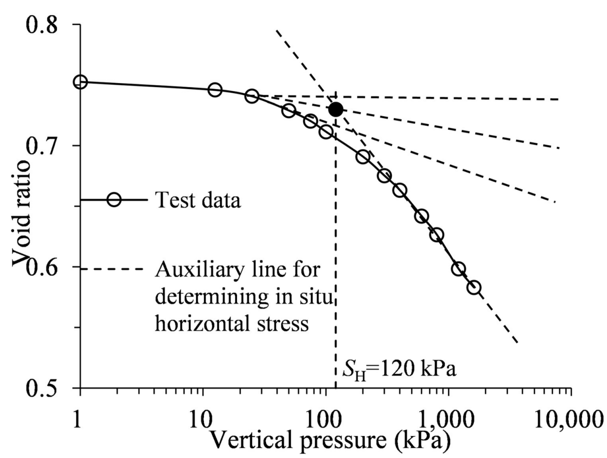

Figure 7. Compression curve of the expansive soil.

The shear strength parameters obtained from BST are the lowest among the test methods, and under flooding conditions, they closely resemble the strength of the slip plane observed in Nanyang expansive soils. As seen in the surface of the triaxial sample (Figure 8 (a)), cracks filled with gray-green clay almost run through the sample, with an inclination of approximately 60°. The sample can be easily split apart with minimal hand pressure, fracturing along the pre-existing crack planes, as shown in Figure 8 (b). These observations indicate that the crack planes in the expansive soil are well developed and steeply inclined, with some nearly perpendicular to the horizontal plane—features that closely align with the shear direction in the BST.

From the analysis above, it is evident that the shear strength characteristics of expansive soil are comprehensively affected by factors such as the in-situ stress state, soil structure, and environmental conditions, particularly the presence of water. Therefore, it is considered that the strength parameters obtained from BST, which account for rainfall infiltration effects, provide a more reasonable basis for use as design parameters in major engineering projects within expansive soil regions.

5. Shear strength parameter selection for stability analysis of expansive soil cut slope

The test results indicate that the shear strength parameters of expansive soil obtained using different test methods can vary significantly. In engineering practice, the strength parameters derived from conventional direct shear or triaxial tests are commonly used in the design of cut slopes. However, these values are considerably higher than those obtained from BST. This discrepancy may explain why the shear strength inferred from field failures of expansive soil cut slopes is often much lower than the peak strength measured in laboratory tests.

Figure 9 depicts an expansive soil cut slope along the Nei-Deng Expressway, with a height of 6.0 m and a

Table 4. Shear strength parameters.

Test methods	Shear strength parameters		Hydraulic condition	
			Non-flooding (Natural moisture content)	Flooding (Saturation)
BST	c/kPa	n	6	6
		Mean	20.1	7.0
		SD	2.5	1.5
		95% CI	[17.5, 22.8]	[5.4, 8.6]
	φ/°	n	6	6
		Mean	11.1	10.9
		SD	1.1	0.9
		95% CI	[9.9, 12.3]	[10.0, 11.9]
DST	c/kPa		50.9	32.7
	φ/°		15.9	13.0
CUT	c/kPa		-	28.4
	φ/°		-	14.3
	c'/kPa		-	12.0
	φ'/°		-	23.7

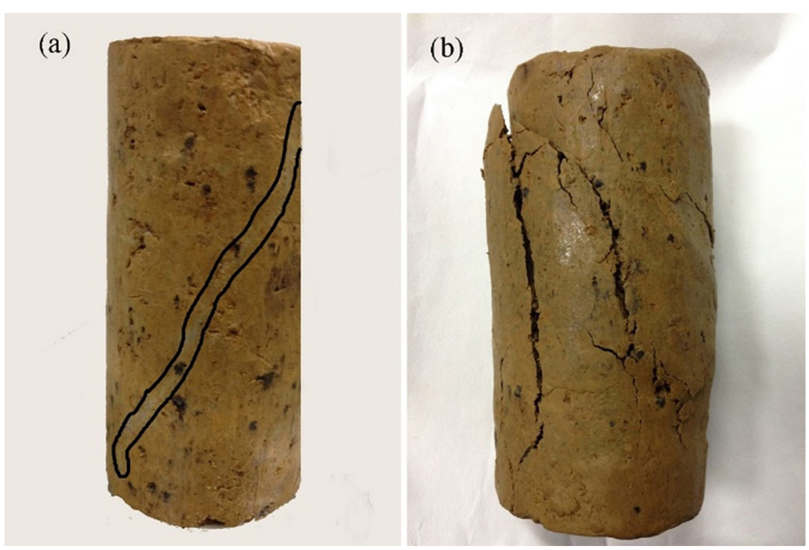

Figure 8. Cracks in triaxial samples: (a) cracks filled with gray-green clay, (b) sample broken apart with a slight push of the hand.

designed slope gradient of 1:1.5. The safety factor calculated using laboratory-derived soil parameters met the design requirements. Nevertheless, during construction, many such slopes experienced collapse or sliding under continuous rainfall, highlighting the limitations of using conventional strength parameters for stability analysis in expansive soil areas.

5.1 Numerical model

Based on the practical expansive soil cut slope, the strength reduction method was employed to analyze its stability using the finite element software ABAQUS. A numerical model of the cut slope was developed with a height of 6.0 m and a slope ratio of 1:1.5 (Figure 10). The distance from the top of the slope to the left boundary was set to 15.0 m, and the distance from the slope toe to the right boundary was also 15.0 m. At the bottom boundary, both horizontal and vertical displacements were fully restrained, while only horizontal displacements were constrained at the lateral boundaries. A static analysis step was then defined, and gravity load was applied to simulate the self-weight of the soil. This initial analysis generated the in-situ stress state, which serves as the starting point for subsequent stability analyses, including simulations of slope failure or progressive collapse.

The mesh density significantly affects both computational accuracy and simulation efficiency. Increasing the number of elements enhances accuracy but also prolongs computation time. Once a certain level of mesh refinement is achieved, further densification results in only marginal gains in accuracy while substantially increasing computational demand. To optimize this trade-off, local grid refinement was conducted through trial calculations within a horizontal range of 5.0 m from both the slope crest and toe, as well as within a vertical depth of 7.0 m from the slope surface.

Research indicates that it is more appropriate to analyze the stability of expansive soil cut slope using a strength zoning approach (Cheng et al., 2011; Liu et al., 2011). According to the Technical Code for Construction in Expansive Soil Areas (GB, 2013), the atmosphere influence depth can be determined based on the soil moisture coefficient (Ψ_w), which is expressed as:

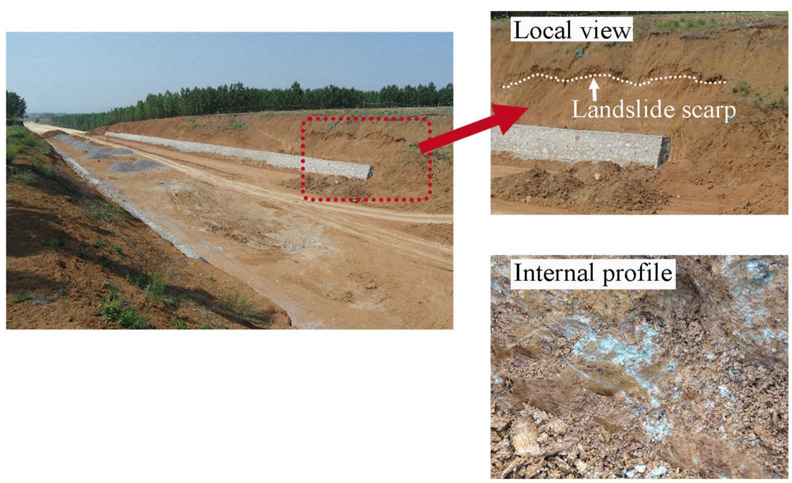

Figure 9. Instability disaster of expansive soil cut slope with a shallow sliding surface, and the internal fresh profile reveals saturation and softening following rainfall.

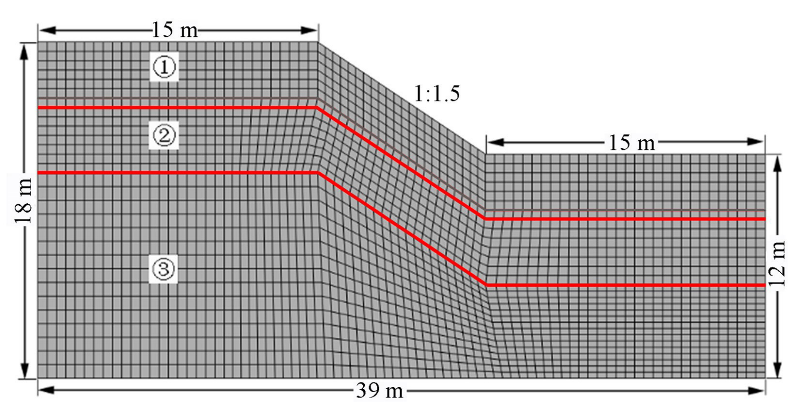

Figure 10. Numerical model.

$$\psi_w = 1.152 - 0.726\alpha - 0.00107\delta \quad (1)$$

where Ψ_w represents the soil moisture coefficient; α represents the ratio of local evaporation power from September to February of the following year to the annual evaporation power (excluding months with an average monthly temperature below 0°C); δ represents the sum of the differences between evaporation power and precipitation in months where the aridity index exceeds 1.0 and the average monthly temperature is above 0°C.

In Nanyang, the monthly mean temperature remains above 0°C year-round. Based on the monthly average evaporation and precipitation data, α was calculated as 0.258 and δ as 165.7. Substituting these values into Equation (1) yields $\Psi_w = 0.8$.

According to GB 50112-2013 (GB, 2013), when ψ_w=0.8, the atmosphere influence depth is 3.5 m, and the layer most significantly influenced by atmospheric conditions is approximately 1.6 m which can be 0.45 times the atmosphere influence depth. Therefore, the expansive soil cut slope was divided into three distinct layers. The atmospheric influence zone was within 3.0 m (layer ①), the transition zone was 3.0~7.0 m (layer ②), and below 7.0 m was considered as an unweathered zone (layer ③).

For numerical modeling, strength parameters obtained under both natural and flooding conditions from each test method were applied to Layer ① to simulate the slope behavior before and after rainfall, respectively. For Layer ②, where the groundwater table is low, only the strength parameters under natural moisture conditions were used. In Layer ③, the strength parameters under natural moisture conditions obtained from DST were adopted.

The Mohr–Coulomb failure criterion was employed in the numerical simulation. The Young's modulus values for Layers ① to ③ were determined as 21.5 MPa, 23.8 MPa, and 24.3 MPa, respectively, based on pressuremeter test results, with a constant Poisson's ratio of 0.3 (Budhu, 2010; Nelson et al., 2015).

5.2 Numerical result analysis

Table 5 presents a comparison of the slope safety factor calculated using strength parameters obtained from different test methods and under various hydraulic conditions. The results reveal that the safety factor under natural moisture conditions is significantly higher than that under flooding conditions. Specifically, the safety factors derived from DST and BST under natural conditions are 1.23 and 1.90 times, respectively, those obtained under corresponding flooding conditions. Moreover, when using DST-derived saturated strength parameters, the safety factor is 1.64 and 2.04 times greater than that calculated using BST-derived parameters under natural and flooding conditions, respectively.

These findings indicate that, based on laboratory-derived strength parameters, the cut slope appears to be highly stable. In practice, the slope remained stable prior to rainfall but experienced failure following rainfall events. This discrepancy highlights the inconsistency between the stability predicted by conventional laboratory tests and the actual field performance.

In contrast, the safety factor calculated using BST-derived parameters decreased from 1.793 under natural conditions to 0.946 under flooding conditions, clearly indicating slope instability after rainfall. This result aligns well with the observed behavior in the field. Given the relatively small variation in internal friction angle, further analysis assuming constant internal friction angle yielded a back-calculated cohesive force of 7.9 kPa under limit equilibrium conditions, which closely matches the 7.0 kPa value obtained from flooding BST tests.

Therefore, it can be concluded that the strength parameters obtained from the BST more accurately reflect the in-situ mechanical behavior of expansive soil.

Figure 11 shows the distribution of the plastic zone in the cut slope, represented by the equivalent plastic strain at integration points, based on strength parameters obtained from BST before and after flooding.

The results reveal that, under natural (pre-flooding) conditions, the plastic zone initiates at the slope toe and gradually extends upward, forming a potential sliding surface at a depth of approximately 5.0 m in an arc-shaped pattern. After flooding, however, the plastic zone develops not only from the slope toe but also from the interface between layer ① (atmospheric influence zone) and layer ② (transition zone) near the toe. The plastic zones rapidly coalesce and progressively extend toward the slope crest, forming a broken-line-shaped sliding surface within a depth of less than 3.0 m.

This behavior can be attributed to the following mechanism: in a homogeneous slope, stress concentration typically initiates at the slope toe, leading to progressive development of the plastic zone from the toe toward the upper part of the slope. However, rainfall infiltration causes near-surface soils to soften, significantly reducing their shear strength. The boundary between softened and partially softened soil becomes a zone of stress concentration, where the induced stress may exceed the reduced shear strength, triggering localized plastic deformation. As the stress redistributes to surrounding areas, the plastic zone expands and eventually connects, leading to slope failure.

Table 5. Safety factors calculated by different test methods and hydraulic conditions.

Conditions	BST		DST		CUT	
	Non-flooding	Flooding	Natural moisture content	Saturation	Total strength	Effective strength
Safety factor	1.793	0.946	3.657	2.946	2.342	1.812

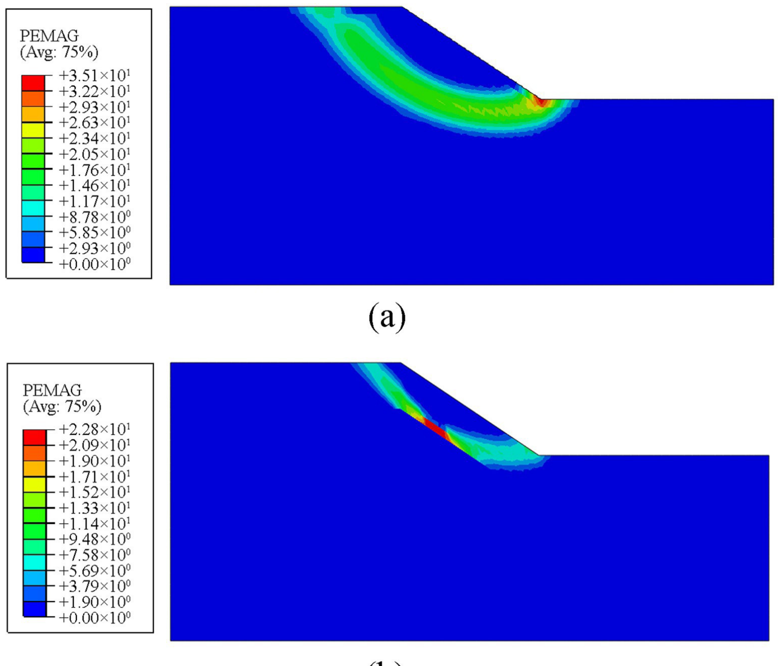

Figure 11. Plastic zone development in the expansive soil cut slope (a) before flooding; (b) after flooding.

6. Conclusion

This study investigates the influence of flooding conditions and test methods on the shear strength parameters of expansive soils, combining in-situ borehole shear tests, laboratory tests, and numerical slope stability analysis. The key finding is that, even under saturated conditions, conventional laboratory-derived strength parameters significantly overestimate the actual shear resistance of expansive soil slopes during rainfall events. This overestimation leads to unrealistically high safety factors and can result in unexpected slope failures. In contrast, shear strength parameters obtained from flooding BST closely align with those measured on actual slip surfaces and yield safety factors that more accurately reflect field instability conditions.

Based on these results, we recommend that shear strength parameters from flooding BST be adopted as the primary input for stability design of cut slopes in expansive soils, particularly in regions subject to seasonal rainfall. When in-situ flooding BST is not feasible due to site or resource constraints, an acceptable alternative is to use residual strength parameters from soils sampled along existing slip surfaces, which exhibit comparable values.

It should be noted that the findings are based on expansive soils from a cut slope in the Nanyang Basin, China, and should be validated on other expansive soils to assess broader applicability. While the study provides valuable insights into shear strength under different test methods and hydraulic conditions, direct monitoring of infiltration, suction, or pore pressure during flooding BSTs was not conducted, limiting the ability to confirm full hydraulic equilibrium or the exact timing of strength reduction. Future work should incorporate real-time hydraulic monitoring and adopt motor-driven, automated shear systems to improve precision, repeatability, and the understanding of hydromechanical behavior in expansive soils, particularly for cut slope stability analysis.

Acknowledgements

The present work was supported by the National Natural Science Foundation of China (Grant numbers 12002121, 41430634), Henan Outstanding Youth Science Foundation (Grant number 242300421153), and Open Research Fund of State Key Laboratory of Geomechanics and Geotechnical Engineering, Institute of Rock and Soil Mechanics, Chinese Academy of Sciences (SKLGME022027).

Declaration of interest

The authors have no conflicts of interest to declare. All co-authors have observed and affirmed the contents of the paper and there is no financial interest to report.

Authors' contributions

Jingjing Li: conceptualization, data curation, visualization, writing – original draft, funding acquisition. Lingwei Kong: conceptualization, methodology, supervision, validation, funding acquisition. Lei Jin: writing – original draft, formal analysis, investigation, methodology. Xinming Li: supervision, validation, writing – review & editing, funding acquisition.

Data availability

The datasets generated analyzed in the course of the current study are available from the corresponding author upon request.

Declaration of use of generative artificial intelligence

This work was prepared without the assistance of generative artificial intelligence (GenAI).

List of symbols and abbreviations

c	Cohesive force
c'	Effective cohesive force
n	Number of tests
nat	Natural moisture content condition
rps	Revolutions per second
sat	Flooding or saturation condition
w_L	Liquid limit
w_P	Plastic limit
A_c	Activity
BST	Borehole shear test
CUT	Consolidated undrained test
DST	Direct shear test
F_s	Free-swell value
G_s	Specific gravity
LI	Liquidity index
PI	Plasticity index
SD	Standard deviation
S_H	In-situ horizontal stress
S_r	Saturation
α	Ratio of local evaporation power from September to February of the following year to the evaporation power of the whole year (excluding months when the average monthly temperature is less than 0°C)
δ	Sum of the difference between evaporation power and precipitation in months with dryness greater than 1.0 and average monthly temperature greater than 0°C
ρ	Density
φ	Internal friction angle
φ'	Effective internal friction angle
Ψ_w	Revolutions per second
ω	Water content
ω_f	Standard absorption moisture content
σ_3	Confining pressure
95% CI	95% Confidence Interval

References

ASTM D2487-17. (2017). *Standard practice for classification of soils for engineering purposes (Unified soil classification system)*. ASTM International, West Conshohocken, PA.

Budhu, M. (2010). *Soil mechanics and foundations* (3rd ed.). John Wiley and Sons.

Chang, J., Xu, Y., Xiao, J., Wang, L., & Jiang, J.Q. (2022). Water-soil chemical mechanism and soil structural stability of expansive soil under the action of acid rain infiltration. *Bulletin of Engineering Geology and the Environment*, 81(10), 438. https://doi.org/10.1007/s10064-022-02933-3.

Cheng, Z.L., Li, Q.Y., Guo, X.L., & Gong, B.W. (2011). Study on the stability of expansive soil slope. *Changjiang Kexueyuan Yuanbao*, 28(10), 102-111. (in Chinese). https://doi.org/10.3969/j.issn.1001-5485.2011.10.019.

Dai, Z.J., Chen, S.X., & Li, J. (2017). *The failure characteristics and evolution mechanism of the expansive soil trench slope* (pp. 196-205). PanAm Unsaturated Soils. https://doi.org/10.1061/9780784481691.020

Dai, Z.J., Huang, K., Chi, Z.C., & Chen, S.X. (2024). Model test study on the deformation and stability of rainfall-induced expansive soil slope with weak interlayer. *Bulletin of Engineering Geology and the Environment*, 83(3), 76. https://doi.org/10.1007/s10064-024-03576-2.

GB 50112-2013. (2013). *Technical code for buildings in expansive soil regions*. China Building Industry Press, Beijing, China (in Chinese).

Handy, R.L., Schmertmann, J.H., & Lutenegger, A.J. (1985). Borehole shear tests in a shallow marine environment. *Strength Testing of Marine Sediments: Laboratory and In-Situ Measurements*. *ASTM Special Technical Publication*, 883, 140-153.

Hou, D., Zhou, Y., & Zheng, X. (2023). Seepage and stability analysis of fissured expansive soil slope under rainfall. *Indian Geotechnical Journal*, 53(1), 180-195. https://doi.org/10.1007/s40098-022-00667-3.

Hou, T.S., Xu, G.L., Shen, Y.J., Wu, Z.Z., Zhang, N.N., & Wang, R. (2013). Formation mechanism and stability analysis of the Houba expansive soil landslide. *Engineering Geology*, 161, 34-43. https://doi.org/10.1016/j.enggeo.2013.04.010.

Jamei, M., Guiras, H., & Olivella, S. (2015). Analysis of slope movement initiation induced by rainfall using the Elastoplastic Barcelona Basic Model. *European Journal of Environmental and Civil Engineering*, 19(9), 1033-1058. https://doi.org/10.1080/19648189.2014.996670.

JTG 3363-2019. (2019). *Specifications for design of foundation of highway bridges and culverts*. China Communications Press, Beijing, China (in Chinese).

JTG 3430-2020. (2020). *Test methods of soils for highway engineering*. China Communications Press, Beijing, China (in Chinese).

JTG C20-2011. (2011). *Code for highway engineering geological investigation*. China Communications Press, Beijing, China (in Chinese).

Kong, L., Li, J., Guo, A., & Zhou, Z. (2017). Influence of loading mode and flooding on in-situ shear strength of expansive soils by borehole shear tests. In *Proc. 19th International Conference on Soil Mechanics and Geotechnical Engineering* (pp. 1197-1200), Seoul. ISSMGE.

Kong, L.W., Zeng, Z.X., Bai, W., & Wang, M. (2018). Engineering geological properties of weathered swelling mudstones and their effects on the landslides occurrence in the Yanji section of the Jilin-Hunchun high-speed railway. *Bulletin of Engineering Geology and the Environment*, 77(4), 1491-1503. https://doi.org/10.1007/s10064-017-1096-2.

Li, J., & Kong, L. (2021). Creep properties of expansive soils under triaxial drained conditions and its nonlinear constitutive model. *Periodica Polytechnica. Civil Engineering*, 65(4), 1269-1278. https://doi.org/10.3311/PPci.18406.

Li, J., Kong, L., & Jin, L. (2024). In-situ creep behavior of expansive soils based on pressuremeter test. *Geotechnical and Geological Engineering*, 42(2), 1209-1222. https://doi.org/10.1007/s10706-023-02614-2.

Liang, C., Wu, Z., Liu, X., Xiong, Z., & Li, T. (2021). Analysis of shallow landslide mechanism of expansive soil slope under rainfall: a case study. *Arabian Journal of Geosciences*, 14(7), 584. https://doi.org/10.1007/s12517-021-06829-6.

Lin, L.S., Jiang, G., Liu, Z.D., & Bai, S.W. (2002). Preliminary study on the strength characteristics of expansive soil and the selection method for shear strength parameters in slope stability analysis. *Guangdong Water Resources and Hydropower*, (1), 9-11. (in Chinese). https://doi.org/10.3969/j.issn.1008-0112.2002.01.003.

Liu, T.H., Shao, Z.Y., & Luan, Y.S. (2011). *Geotechnical engineering techniques and examples*. China Building Industry Press (in Chinese).

Luo, X., Kong, L., Yan, J., Gao, Z., & Tian, S. (2024). In-situ mechanical property and mechanism analysis of shallow expansive soil under the influence of water content and fissures. *KSCE Journal of Civil Engineering*, 28(10), 4281-4292. https://doi.org/10.1007/s12205-024-1440-6.

Lutenegger, A.J., & Hallberg, G.R. (1981). Borehole shear test in geotechnical investigations. *Laboratory Shear Strength of Soil. ASTM Special Technical Publication*, 740, 566-578.

Marsland, A., & Randolph, M.F. (1977). Comparisons of the results from pressuremeter tests and large in situ plate tests in London clay. *Geotechnique*, 27(2), 217-243. https://doi.org/10.1680/geot.1977.27.2.217.

Nelson, J.D., & Miller, D.J. (1992). *Expansive soils: problems and practice in foundation and pavement engineering*. John Wiley and Sons.

Nelson, J.D., Chao, K.C., Overton, D.D., & Nelson, E.J. (2015). *Foundation engineering for expansive soils*. John Wiley and Sons. https://doi.org/10.1002/9781118996096.

Ng, C.W.W., & Zhan, L.T. (2007). Comparative study of rainfall infiltration into a bare and a grassed unsaturated expansive soil slope. *Soil and Foundation*, 47(2), 207-217. https://doi.org/10.3208/sandf.47.207.

Ng, C.W.W., Zhan, L.T., Bao, C.G., Fredlund, D.G., & Gong, B.W. (2003). Performance of an unsaturated expansive soil slope subjected to artificial rainfall infiltration. *Geotechnique*, 53(2), 143-157. https://doi.org/10.1680/geot.2003.53.2.143.

Niu, G., Sun, D., Kong, L., Shao, L., Wang, H., & Wang, Z. (2024). Investigation into the shear strength of a weakly expansive soil over a wide suction range. *Acta Geotechnica*, 19(5), 3059-3073. https://doi.org/10.1007/s11440-024-02246-7.

Pei, P., Zhao, Y.L., Ni, P.P., & Mei, G.X. (2020). A protective measure for expansive soil slopes based on moisture content control. *Engineering Geology*, 269, 105527. https://doi.org/10.1016/j.enggeo.2020.105527.

Shi, B., Jiang, H.T., Liu, Z.B., & Fang, H.Y. (2002). Engineering geological characteristics of expansive soils in China. *Engineering Geology*, 67(1-2), 63-71. https://doi.org/10.1016/S0013-7952(02)00145-X.

Xu, L., Dai, F., Chen, J., Iqbal, J., & Qu, Y. (2014). Analysis of a progressive slope failure in the Xiangjiaba reservoir area, *Southwest China. Landslides*, 11(1), 55-66. https://doi.org/10.1007/s10346-012-0373-1.

Yang, G.L., Teng, K., & Xie, L.F. (2014). Experimental study of direct shear and in situ clipper on strength of expansive soil. *Journal of Central South University*, 45(6), 1952-1959.

Yu, Y.T., Zheng, J.G., Liu, Z.H., & Zhang, J.W. (2016). Borehole shear test and its application to loess. *Yantu Lixue*, 37(12), 3635-3641. (in Chinese).

Zhan, L.T. (2003) *Field and laboratory study of an unsaturated expansive soil associated with rain-induced slope instability* [thesis]. The Hong Kong University of Science and Technology. Retrieved in August 20, 2024, from http://respository.ust.hk/ir/Record/1783.1-1596

Zhan, T.L., Ng, C.W.W., & Fredlund, D.G. (2007). Field study of rainfall infiltration into a grassed unsaturated expansive soil slope. *Canadian Geotechnical Journal*, 44(4), 392-408. https://doi.org/10.1139/t07-001.

Zhang, H., Yang, J., Wang, L., Xu, Y., Lan, S., Luo, J., & Chang, Z. (2023). Experimental and numerical investigation on failure mechanism of expansive soil subgrade slope. *Scientific Reports*, 13(1), 19795. PMid:37957240. https://doi.org/10.1038/s41598-023-46727-3.

Zhang, J.R., Niu, G., Li, X.C., & Sun, D.A. (2020). Hydro-mechanical behavior of expansive soils with different dry densities over a wide suction range. *Acta Geotechnica*, 15(1), 265-278. https://doi.org/10.1007/s11440-019-00874-y.